Available online at www.sciencedirect.com
ScienceDirect
International Journal of Solids and Structures 45 (2008) 478–496
INTERNATIONAL JOURNAL OF SOLIDS AND STRUCTURES
www.elsevier.com/locate/ijsolstr

An analytic model for the response to water blast of unsupported metallic sandwich panels

R.M. McMeeking [a,b], A.V. Spuskanyuk [a,*], M.Y. He [b], V.S. Deshpande [a], N.A. Fleck [c], A.G. Evans [a,b]

[a] *Mechanical Engineering Department, University of California, Santa Barbara, CA 93106, USA*
[b] *Materials Department, University of California, Santa Barbara, CA 93106, USA*
[c] *Engineering Department, Cambridge University, Trumpington Street, Cambridge CB2 1PZ, UK*

Received 2 April 2007; received in revised form 3 August 2007
Available online 19 August 2007

Abstract

A prior assessment of the response of a metallic sandwich panels to water blast has identified soft and strong core responses and outlined the advantages of softness. Ensuing analysis has provided mechanism maps that distinguish these responses. The present article extends these assessments by developing an analytic model for the wet face response, inclusive of fluid/structure interaction, that can be used for a wide range of core topologies. The model addresses cavitation and incorporates the momentum of reconstituted water attached to the wet face. It assumes a transient dynamic strength of the core associated with dynamic buckling. The model includes coefficients that have been independently characterized using numerical simulations. The fidelity of the analytic model has also been assessed using simulations. The results reveal that analytic predictions of the wet face velocities are quite accurate for most of the soft cores examined. The implication is that the models may be used as reliable input to panel-level simulations for predicting such metrics as the reaction forces and the displacements. Discrepancies arise for strong cores with relatively large push back stress, and for systems with very thin wet faces, suggesting that embellishments are required for panels incorporating such features.
© 2007 Elsevier Ltd. All rights reserved.

Keywords: Blast loading; Finite element simulations; Sandwich structures; Fluid–structure interaction; Dynamic core strength

1. Introduction

Insights regarding the response of metallic sandwich panels to water blast have been gained by recent assessments of the fluid/structure interaction (FSI) by Deshpande and Fleck (2005), Xue and Hutchinson (2004), Fleck and Deshpande (2004), Liang et al. (2007), Hutchinson and Xue (2005), Tilbrook et al. (2006). Most crucial has been the discovery of soft and strong core responses when the panel is subjected

* Corresponding author. Tel.: +1 805 893 7278.
E-mail address: spusk@engineering.ucsb.edu (A.V. Spuskanyuk).

0020-7683/$ - see front matter © 2007 Elsevier Ltd. All rights reserved.
doi:10.1016/j.ijsolstr.2007.08.003

Nomenclature

List of symbols

c_{pl}	plastic wave speed of base material
c_w	sound speed in water
E, E_T	Young's modulus and plastic tangent modulus of base material
H_c	height of the core
h_{wet}, h_{dry}	thickness of the wet and dry faces, respectively
I_{tot}	momentum of the free-standing sandwich plate
m_{wet}, m_{dry}, m_{core}	mass per unit area of wet, dry faces and core, respectively
M_{wet}, M_{dry}	effective mass per unit area of wet and dry faces, respectively
p	fluid pressure
p_c	cavitation pressure
p_0	peak pressure of free field impulse
t	time
t_0	characteristic time of incident pressure pulse
t_1	first cavitation time
t_c	time of cavitation at the wet face
t_{common}	time when the wet and dry faces of the sandwich panel attain a common velocity $v_{wet} = v_{dry}$
t_{peak}	wet face peak velocity time
t_{pulse}	pulse time, after which core buckles and its compressive strength reduces
t_x	cavitation time at position x
v	velocity of the fluid
v_r	velocity of the fluid at the instant of its cavitation
$\widehat{v}_{peak}$	wet face peak velocity
$\widehat{v}_{wet}$	wet face velocity at the instant of cavitation at the wet face i.e. $t = t_c$
v_{wet}, v_{dry}	velocity of the wet and dry faces, respectively
$\dot{v}_{dry}$	acceleration of the dry face
x, X	original and current position of material points of water; the water occupies $x < 0$
x_e	reconstitution wave front location
x_{cav}	location of the breaking front
x^0_{cav}	location of the breaking front at the instant $t = t_c$
β	fluid–structure interaction parameter
$\dot{\varepsilon}_p$	plastic strain rate
ρ	density of the base material
$\bar{\rho}$	relative density of the core
ρ_w	density of the water
$\widehat{\sigma}$	wet face stress
σ_Y	yield strength of the base material
σ^c_{YD}	dynamic yield strength of the core
σ_{pulse}, σ_{ss}	effective dynamic strength of the core before and after t_{pulse}, respectively
ψ, ϕ, χ	empirical coefficients

to a high impulse fluid-interaction pressure or an impulsive loading on its wet face (Liang et al., 2007). The occurrence of soft or strong core behavior is dependent on such factors as the dynamic strength of the core, its thickness and the magnitude of the impulse (Tilbrook et al., 2006). By design of the core to elicit a soft response, all relevant performance metrics are beneficially affected. Namely, the forces transmitted to the supports, the panel center deflection and the plastic strains induced in the faces are all reduced (Liang et al., 2007; Tilbrook et al., 2006). However, the soft design must assure that the front face does not slap into the back, e.g. by ensuring that the core is tall, so that the wet face is either arrested before a slap occurs, or its velocity

equalizes with that of the back face prior to any collision. If a slap does occur, the ordering of the performance inverts according to Tilbrook et al. (2006).

Liang et al. (2007) and Tilbrook et al. (2006) found that the relative velocity transients of the wet and dry faces are qualitatively different for soft and strong responses (Fig. 1), which allows for a distinction of the two behaviors. Upon sustaining the impulse, the wet face rapidly accelerates to a maximum velocity, just before water cavitation commences. Thereafter, the core imposes a push back stress, causing the wet face to decelerate. Simultaneously, the back face accelerates. The magnitude of the accelerations depend upon the dynamic strength of the core, as well as upon the pressure loading by the cavitated water after it has reattached to the wet face.

If the accelerations and decelerations are sufficiently large, the wet and dry face velocities converge to a common velocity (Xue and Hutchinson, 2004) and a strong response arises (Liang et al., 2007). Subsequently, both faces decelerate together and arrest. Conversely, if the dry face arrests before acquiring the velocity of the wet face, the subsequent response is soft and is quite different.

A model that distinguishes soft and strong responses is contingent upon a comprehensive understanding of the factors controlling the velocities of the faces. Tilbrook et al. (2006) have developed the associated mechanics for impulsively loaded panels with cores that crush at constant dynamic strength. Examples suggest that the soft behavior occurs over a limited range of geometries, core strengths and blast impulse. It remains to develop analogous solutions for panels subject to water blast (with associated FSI considerations) and to extend the ideas to panels with structured prismatic cores. The primary objective of this article is to establish an analytical model for the velocity characteristics of the faces of unsupported panels, representative of the central segment of an edge supported panel prior to the deceleration of the dry face caused by the constraint imposed by the edge supports (Deshpande and Fleck, 2005; Fleck and Deshpande, 2004; Liang et al., 2007; Tilbrook et al., 2006).

To attain this objective, the article includes the following elements. (i) The constituent properties of representative prismatic cores are summarized. (ii) An analytical model governing the velocities of the wet face is developed, by envisaging it as a solid plate that interacts with a homogenized core only through its dynamic strength, σ^{c}_{YD}. (iii) Numerical unit cell calculations are conducted for the I-core configuration. These are used

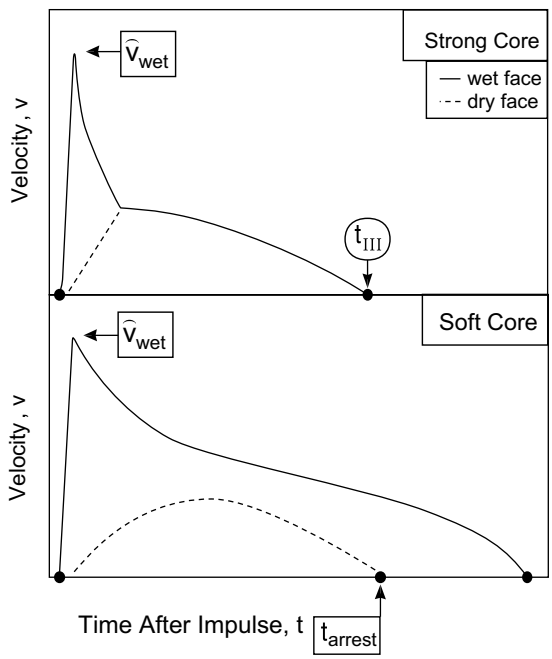

Fig. 1. Trends in the wet and dry face velocities for a sandwich panel supported on the dry face and subjected to a water blast. (a) Strong response in which the velocities of the two faces converge to a common value and then decelerate together. (b) Soft response in which the dry face velocity always exceeds that for the wet face.

Table 1
The four cases of steel I-core sandwich beams examined by numerical simulation and the parameters ascertained by fitting to the analytic model

Case		I	II	III	IV
Core relative density	$\bar{\rho}$ (%)	1.33	4.00	1.33	1.33
Wet face thickness	h_{wet} (mm)	8.0	8.0	3.2	8.0
Face thickness ratio	h_{dry}/h_{wet}	1	1	4	1
Core thickness	H_c (m)	0.3	0.1	0.3	0.3
Peak pressure	p_0 (MPa)	100	100	100	200
Peak velocity	$\widehat{v}_{peak}$ (m/s)	67.1	61.7	95.0	136.7
Pulse time	t_{pulse} (ms)	0.31	0.175	0.25	0.30
Dynamic yield strength	σ_Y (MPa)	341	363	348	356
Core strength	σ_{pulse} (MPa)	4.5	14.6	4.7	4.7
	σ_{ss} (MPa)	0.33	1.28	0.38	0.40
Coefficients	ψ	1.0	1.0	1.0	1.0
	χ	0.07	0.09	0.08	0.09
	ϕ	1.0	1.8	0.8	1.0

to calibrate coefficients in the analytic model, as well as assess its fidelity. For this purpose, results are presented for the four cases elaborated in Table 1, which embrace the expected range of designs and impulse levels. It will be shown that case II represents a strong core while all others are soft. That is, for cases I, III and IV, the wet face velocity always exceeds that for the dry face (Fig. 1): whereas, for case II, the two faces acquire a common velocity prior to arrest.

2. Synopsis of core response

Ferri et al. (2006) have characterized experimentally the dynamics of I-cores subject to constant velocity imposed on the front (wet) face with rigid support of the back (dry) face. The characterization has been conducted for material properties representative of a stainless steel that exhibits both strain and strain-rate hardening (Stout and Follansbee, 1986; Liu and Guo, 2000; Zok et al., 2004). The observed, typical front (wet) and rear (dry) face stress versus time histories of an I-core are sketched in Fig. 2 and display the following principal characteristics. (i) During an initial phase (for times $t < t_{pulse}$), the wet face and dry faces stresses are constant with the wet face stress $\widehat{\sigma}$ exceeding the dry face stress σ_{pulse} and (ii) at $t = t_{pulse}$, the core dynamically buckles and subsequently both the wet and dry face stresses are approximately constant at a value $\sigma_{ss} < \sigma_{pulse} < \widehat{\sigma}$. We

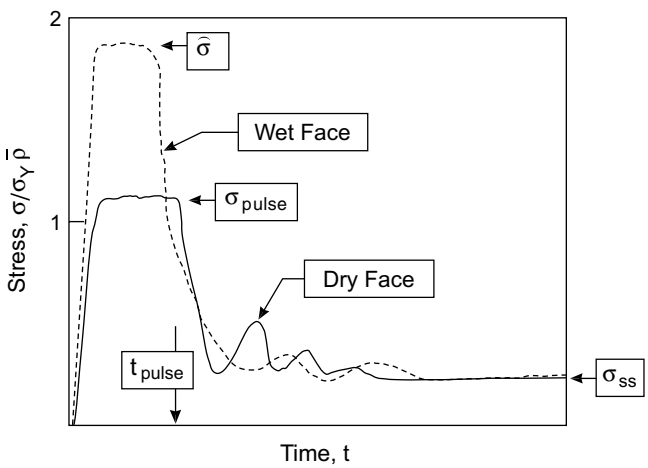

Fig. 2. Illustration of the time variation of the core strength. The wet face strength includes an inertial contribution. The sudden drop in strength at time t_{pulse} coincides with the arrival of the buckle-wave at the dry face.

summarize these characteristic parameters for an I-core constructed from a solid of density ρ, Young's modulus E, dynamic initial yield strength σ_Y and a linearly hardening plastic response with tangent modulus E_T.

The *initial stress* transmitted through the core to the dry face, when rigidly supported, is independent of the front face velocity, and is given by Ferri et al. (2006) as

$$\frac{\sigma_{\text{pulse}}}{\sigma_Y \bar{\rho}} = \psi, \tag{1}$$

where the coefficient, $\psi \approx 1$, an outcome determined empirically by Ferri et al. (2006) from the experiments and confirmed in computations as discussed below, and $\bar{\rho}$ is the relative density of the core. In that sense, ψ is demonstrated to be independent of geometry. When the plastic wave first impinges on the dry face after it has traveled from the wet face, the core plastically buckles and both the wet and dry face stresses drop quite abruptly at a *pulse time*, t_{pulse} given by Xue and Hutchinson (2004) and Ferri et al. (2006) as

$$t_{\text{pulse}} = \phi H_c / c_{\text{pl}}. \tag{2}$$

Numerical calculations indicate, with the exception of one case, that the coefficient, ϕ, is slightly greater than unity, confirming that t_{pulse} is just greater than the time taken for the plastic wave to traverse the core of height H_c at a speed $c_{\text{pl}} \equiv \sqrt{E_T/\rho}$. The discrepancy in the remaining case is not large, but core collapse occurs sooner than predicted by transit of the plastic wave. At time $t > t_{\text{pulse}}$, the strength of the core after it has buckled (equal wet and dry face stresses) is given by Ferri et al. (2006) as:

$$\frac{\sigma_{\text{ss}}}{\sigma_Y \bar{\rho}} = \chi, \tag{3}$$

where the coefficient, $\chi \approx 0.08$. Thus, three non-dimensional parameters dictate the core dynamics (ψ, ϕ, χ) and these are typically determined from numerical calculations or experiment.

To establish a model connecting these strength characteristics to the face velocities, the wet and dry face motions can be analyzed separately, by envisaging them as solid plates that interact with a core only through its dynamic strength. The model for the wet face velocity is addressed in Section 3, with additional details given in Appendix A. Three salient metrics governing the response are ascertained: the maximum velocity acquired by the face, the subsequent rate of deceleration and the transmitted momentum. Approximate formulae for the velocity and impulse obtained from linearization of the governing equations are presented in Appendix B. The fidelity of each aspect of the model is examined through the numerical simulations described in Section 4.

3. A lumped mass model for the response of a free-standing sandwich panel

Consider a sandwich plate comprising rigid wet and dry faces of mass per unit area m_{wet} and m_{dry}, respectively, and a compressible core of mass per unit area m_{core}. Following Tilbrook et al. (2006) we employ a lumped mass approximation with the mass of the core assumed to be distributed equally and uniformly over the wet and dry face sheets. Thus, the effective masses per unit area of the wet and dry faces are

$$M_{\text{wet}} = m_{\text{wet}} + m_{\text{core}}/2 \tag{4a}$$

and

$$M_{\text{dry}} = m_{\text{dry}} + m_{\text{core}}/2, \tag{4b}$$

respectively. Further, we neglect any strengthening of the core due to micro-inertial or shock wave effects and assume that the transverse compressive strength σ^c_{YD} loads the dry face and decelerates the wet face. However, we shall account for the dynamic buckling of the core by assuming time-dependent core strength specified as

$$\sigma^c_{YD} = \begin{cases} \sigma_{\text{pulse}} & t \leqslant t_{\text{pulse}} \\ \sigma_{\text{ss}} & t > t_{\text{pulse}} \end{cases}. \tag{5}$$

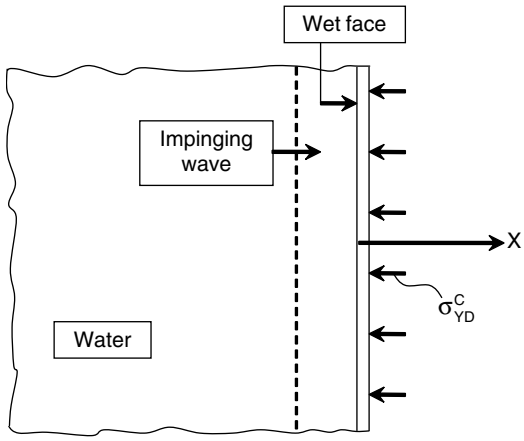

Fig. 3. The co-ordinate system employed in the analysis of the wet face on a plastic foundation impinged by the water blast wave.

Since each face is modeled as rigid, their thickness does not enter the calculation, and the origin is taken as the wet face of the sandwich plate, while water of density ρ_w occupies the region $x \leqslant 0$ (Fig. 3). The sandwich panel is impacted by a pressure wave traveling in the positive x direction at a speed c_w. Upon use of the usual Taylor (1963) assumption that the pressure profile of the incoming shock wave has decaying exponential shape, with time constant t_0, the incoming pressure wave that impinges on the structure at time $t = 0$ is written as

$$p = p_0 e^{-(t - x/c_w)/t_0}. \tag{6}$$

Note that this form, used widely by Deshpande and Fleck (2005), Xue and Hutchinson (2004), Fleck and Deshpande (2004), Liang et al. (2007), Hutchinson and Xue (2005), Tilbrook et al. (2006), Taylor (1963), omits some of the details of pulse shapes associated with underwater explosions. The effects of these details in an impulsive loading of a single degree of freedom elastic–plastic system have been assessed by Li and Meng (2002). The wave defined in Eq. (6) interacts with the sandwich panel, reflecting from it; the subsequent pressure distribution in the water depends on the motion of the sandwich panel and can be summarized as follows. The motion of the wet face of the sandwich plate causes the reflected wave to comprise a rarefaction component (Taylor, 1963). This rarefaction leads the water to first cavitate at time $t = t_1$ some distance away from the interface between the water and the sandwich plates (Fig. 4a) (Deshpande and Fleck, 2005; Xue and Hutchinson, 2004; Bleich and Sandler, 1970). As given by Kennard (1943), two breaking fronts (N.B. these are not acoustic waves) that have been shown to travel supersonically emanate from this cavitation plane: the first travels away from the structure while the second approaches it (Fig. 4b) (Deshpande and Fleck, 2005; Liang et al., 2007; Bleich and Sandler, 1970); in Fig. 4d, the breaking front has just reached the wet face. The breaking front that travels towards the sandwich plate reflects from its wet face as a reconstitution wave that reattaches water to the sandwich plate (Fig. 4e), according to Deshpande and Fleck (2005), Liang et al. (2007). Note that this reconstitution front never catches up with the first breaking front (Deshpande and Fleck, 2005; Liang et al., 2007; Kennard, 1943). We now present an analysis for the motion of the wet face of the sandwich plate that takes into account these features.

3.1. The governing equations for the motion of the wet face

We derive approximate relations for the velocity of the wet face by analyzing the motion of a rigid plate of mass per unit area M_{wet} on a plastic foundation with strength σ^c_{YD} (Fig. 3). The plate is loaded by the incoming blast wave. Taylor (1963) calculated the response of a free-standing rigid plate subjected to a blast wave of the form (6). He found that the response is dictated by a single non-dimensional group, termed the fluid–structure interaction parameter $\beta = \rho_w c_w t_0 / M_{wet}$. Subsequent modifications (Xue and Hutchinson, 2004; Liang et al.,

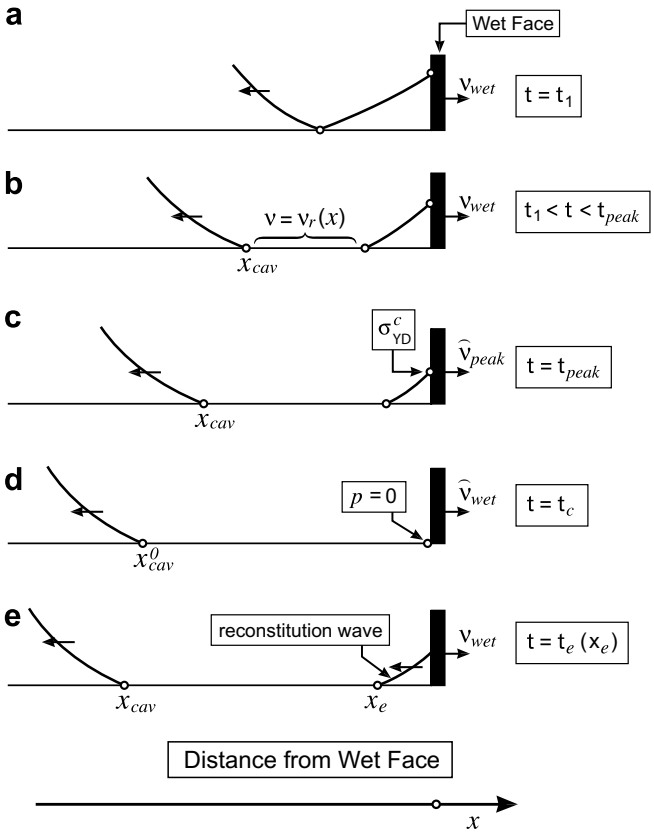

Fig. 4. Sketch of the spatial variation in the fluid pressure at selected times. (a) First cavitation at $t = t_1$, which occurs at some stand-off from the wet face. (b) Just afterwards, cavitated pool spreads due to a breaking wave front at x_{cav} that travels to the left and another one that travels to the right. The water in between travels at constant velocity v_r. (c) At time $t = t_{peak}$, the pressure in the fluid at the wet face has fallen to a value exactly equal to the core strength, σ^c_{YD}, and so the wet face has reached its maximum velocity, $\hat{v}_{peak}$. (d) Very soon thereafter, at time $t = t_c$, the rightmost breaking front reaches the wet face and thus the pressure there falls to zero. (e) Because the wet face is now decelerating, the breaking front reflects from the wet face as a reconstitution wave which travels to the left and creates a layer of attached water.

2007) to the Taylor model for a rigid plate on a plastic foundation give the pressure in the water between the reflected wave front and the wet face as

$$p(x,t) = p_0\left[e^{\frac{x-c_w t}{c_w t_0}} - \left(\frac{2\beta}{1-\beta} + \frac{\sigma^c_{YD}}{p_0}\right)e^{\frac{-\beta(x+c_w t)}{c_w t_0}} + \frac{1+\beta}{1-\beta}e^{\frac{-(x+c_w t)}{c_w t_0}} + \frac{\sigma^c_{YD}}{p_0}\right] \tag{7}$$

for $-tc_w \leqslant x \leqslant 0$. The pressure given by (7) is valid until the water first cavitates. Here, we assume that the water can sustain no tension and thus the cavitation pressure $p_c = 0$. Cavitation initiates at time t_1 such that the minimum value of $p(x,t_1)$ vanishes, with the minimization conducted over all x and $p(x,t_1)$ given by (7). The pressure distribution at this instant is sketched in Fig. 4a.

Prior to cavitation, the velocity in the fluid, between the reflected wave front and the wet face, is given by

$$v(x,t) = \frac{p_0}{\rho_w c_w}\left[e^{\frac{x-c_w t}{c_w t_0}} + \left(\frac{2\beta}{1-\beta} + \frac{\sigma^c_{YD}}{p_0}\right)e^{\frac{-\beta(x+c_w t)}{c_w t_0}} - \frac{1+\beta}{1-\beta}e^{\frac{-(x+c_w t)}{c_w t_0}} - \frac{\sigma^c_{YD}}{p_0}\right]. \tag{8}$$

After first cavitation, $t > t_1$, two breaking waves diverge. The water remains cavitated between these two waves, see Fig. 4b. For later use, the location of the outgoing breaking front is labeled $x_{cav}(t)$. Eq. (7) remains valid in the uncavitated regions (where the pressure is positive) *even after cavitation has commenced* somewhere in the water. Consequently, the cavitation time $t_x(x)$ at a location x in the water is obtained by setting the

pressure to zero in (7) and solving the implicit equation $p(x,t_x)=p_c=0$. Comparing Eqs. (7) and (8), we observe that the velocity of the fluid at the instant of its cavitation ($p(x,t_x)=0$) is given as

$$v_r(x)=\frac{2p_0}{\rho_w c_w}e^{\frac{x-c_w t_x(x)}{c_w t_0}}. \tag{9}$$

Momentum conservation dictates that this fluid velocity remains constant as long as the fluid remains in a cavitated state. Noting that the pressure in the fluid at $x=0$ decreases with increasing time, we deduce that the wet face will acquire its peak velocity when $p(x=0,t_{peak})=\sigma^c_{YD}$. The pressure distribution at this instant is sketched in Fig. 4c. Thereafter, the push back stress due to the core decelerates the wet face. The time t_{peak} is obtained by setting $p(x=0,t_{peak})=\sigma^c_{YD}$ in Eq. (7) and is given as

$$t_{peak}=\frac{t_0}{\beta-1}\ln\left(\beta+\frac{1-\beta}{2}\frac{\sigma^c_{YD}}{p_0}\right). \tag{10}$$

Prior to t_{peak} there is no cavitation at $x=0$. Continuity thus dictates that the velocity of the wet face is equal to that of the fluid at $x=0$, and consequently the corresponding peak velocity of the wet face follows when Eq. (10) is inserted for t into (8) giving

$$\widehat{v}_{peak}=\frac{2p_0}{\rho_w c_w}\left\{\left(\beta+\frac{1-\beta}{2}\frac{\sigma^c_{YD}}{p_0}\right)^{\frac{1}{1-\beta}}-\frac{\sigma^c_{YD}}{2p_0}\right\}. \tag{11}$$

The above analysis for the motion of the wet face can be continued until the breaking front reaches the wet face of the sandwich plate and the fluid cavitates there at a time $t_c=t_x(0)$, where t_c is obtained by solving Eq. (7) as $p(0,t_c)=0$. The associated wet face velocity, $\widehat{v}_{wet}$, is obtained by setting $x=0$ and $t=t_c$ in Eq. (9). At the instant $t=t_c$, the location of the outgoing breaking front is labeled as $x_{cav}(t_c)=x^0_{cav}$. The pressure vanishes throughout the water except for $x<x^0_{cav}$, see Fig. 4d.

Now consider the response for $t>t_c$. Deceleration of the wet face continues at time $t=t_c$ and results in the breaking front being reflected as a reconstitution wave, which travels from the wet face into the fluid, with wavefront located at $x_e(t)$. Consequently, cavitation at the wet face does not persist for finite time, and continuity of displacement and velocity between the water at $x=0$ and the wet face is unbroken. Based on the assumption that strains in the uncavitated water are negligible, continuity at the wet face and across the reconstitution front located at x_e gives (see Appendix A)

$$v_{wet}(t)=v_r(x_e)+\frac{dv_r(x_e)}{dx_e}\frac{dx_e}{dt}[t-t_x(x_e)], \tag{12}$$

where v_{wet} is the current velocity of the wet face and x_e is the current location of the reconstitution front measured in the undeformed configuration. Further, we assume that the velocity of the water within the reconstituted zone spanning $x_e\leqslant x\leqslant 0$ is spatially uniform and equal to v_{wet}. Then momentum conservation provides (see Appendix A)

$$\frac{d}{dt}\{[M_{wet}-\rho_w x_e(t)]v_{wet}(t)\}+\rho_w v_r(x_e)\frac{dx_e}{dt}=-\sigma^c_{YD}. \tag{13}$$

For a realistic set of parameters $t_{pulse}\gg t_c$. Thus, the push back strength is a constant at least up to the instant that the breaking front reaches the wet face. Consequently, the motion of the front face is obtained in the following three regimes:

(i) For $t<t_c$, the wet face velocity v_{wet} is given by Eq. (8) with $x=0$.
(ii) For $t_c<t\leqslant t_{pulse}$, we numerically integrate Eqs. (12) and (13) with $\sigma^c_{YD}=\sigma_{pulse}$ and initial conditions $v_{wet}=\widehat{v}_{wet}$ and $x_e=0$ at $t=t_c$.
(iii) For $t>t_{pulse}$, Eqs. (12) and (13) are again employed but now with $\sigma^c_{YD}=\sigma_{ss}$ and initial conditions $v_{wet}=v_{wet}(t_{pulse})$ and $x_e=x_e(t_{pulse})$ as obtained at the end of regime (ii) above.

A schematic of the resulting pressure after the reconstitution wave has set in is given in Fig. 4e.

3.2. The governing equations of motion for the dry face

The above analysis for the wet face is valid until the time t_{common} when the wet and dry faces of the sandwich panel attain a common velocity $v_{\text{wet}} = v_{\text{dry}}$. The time t_{common} is evaluated by examining the motion of the dry face and comparing it with that of the wet face. Since the wet face is decelerating when $t > t_{\text{peak}}$ and the dry face is accelerating after it commences motion, a common velocity will always be achieved after sufficient time. However, slap may intervene if the core is not tall. The lumped mass approximation dictates that the acceleration of the dry face is given as

$$\dot{v}_{\text{dry}} = \sigma^{\text{c}}_{\text{YD}}/M_{\text{dry}} \tag{14}$$

with initial conditions $v_{\text{dry}} = 0$ at $t = 0$ and $\sigma^{\text{c}}_{\text{YD}}$ specified by Eq. (5).

The analyses of Sections 3.1 and 3.2 together give the momentum of the free-standing sandwich plate (including that of the attached water) as

$$I_{\text{tot}} = [M_{\text{wet}} - \rho_{\text{w}} x_e(t)] v_{\text{wet}}(t) + \int_0^t \sigma^{\text{c}}_{\text{YD}}\, \mathrm{d}t = [M_{\text{wet}} - \rho_{\text{w}} x_e(t)] v_{\text{wet}}(t) + M_{\text{dry}} v_{\text{dry}}(t). \tag{15}$$

After sufficient time has passed, the wet and dry faces will reach a common velocity. This event can occur through the processes of deceleration and acceleration of the wet and dry faces, in which case core compression will cease. An alternative possibility is that the wet face slaps into the dry face because the core has been completely crushed. In either case, the sandwich panel will thereafter travel with a uniform and constant velocity consistent with the prior panel momentum. Because the panel is traveling at constant velocity, the pressure in the attached layer adjacent to the wet face will be equal to zero, implying that the water there has cavitated once more. The resulting momentum in the panel can be inferred to be $M_{\text{wet}} v_{\text{wet}}(t_{\text{common}}) + M_{\text{dry}} v_{\text{dry}}(t_{\text{common}})$. Thereafter, the attached layer and the free-standing sandwich panel are effectively decoupled and will remain so.

Approximate closed form expressions for v_{wet}, accurate to first order in $\sigma^{\text{c}}_{\text{YD}}/p_0$, are presented in Appendix B and are subsequently compared with the exact numerically integrated solutions.

3.3. Effect of core strength and lumped mass approximation

We aim to understand (i) the effect of lumping the core mass into the faces and (ii) the effect of the push back stress. For this assessment we employ the strong core situation (case II) outlined in Table 1, with the mass per unit area of the wet face and core estimated, respectively, as $m_{\text{wet}} = h_{\text{wet}}\rho$ and $m_{\text{core}} = H_{\text{c}}\bar{\rho}\rho$, given a wet face of steel with thickness h_{wet} and a density of steel taken to be $\rho = 8000\ \text{kgm}^{-3}$. Case II is utilized for this study as it imposes the largest core push back, and so emphasizes the effects of the core strength. The parametric study presented in Fig. 5 uses the following four cases with $\sigma^{\text{c}}_{\text{YD}}$ taken to be constant, i.e. we specify that $\sigma^{\text{c}}_{\text{YD}}$ is time invariant and do not allow for the switch in the core strength from σ_{pulse} to σ_{ss} at $t = t_{\text{pulse}}$:

(i) The push back stress $\sigma^{\text{c}}_{\text{YD}} = \sigma_{\text{pulse}} = 14.6$ MPa and core mass are accounted for using the lumped mass approximation, i.e. M_{wet} is given by Eq. (4a) and thus the fluid–structure interaction parameter $\beta \equiv \rho_{\text{w}} c_{\text{w}} t_0 / M_{\text{wet}}$ equals 1.88.
(ii) The push back stress $\sigma^{\text{c}}_{\text{YD}} = \sigma_{\text{pulse}} = 14.6$ MPa and the core mass is neglected, i.e. $M_{\text{wet}} = m_{\text{wet}}$ and thus $\beta = 2.34$. This is referred to as the Taylor result, consistent with one obtained by Fleck and Deshpande (2004).
(iii) The push back stress is neglected ($\sigma^{\text{c}}_{\text{YD}} = 0$) and the core mass is accounted for using the lumped mass approximation, i.e. M_{wet} is given by Eq. (4a) and $\beta = 1.88$.
(iv) The push back stress and core mass are both neglected (i.e. $\sigma^{\text{c}}_{\text{YD}} = 0$ and $M_{\text{wet}} = m_{\text{wet}}$ giving $\beta = 2.34$).

Note that cases (iii) and (iv) reduce to the original Taylor (1963) analysis.

Results are presented in Fig. 5 for the residual velocity v_{r} in the cavitated water at $t = t_{\text{c}}$ and the cavitation time t_x as a function of the location x. Among these examples, a spread in the predicted water velocity is only

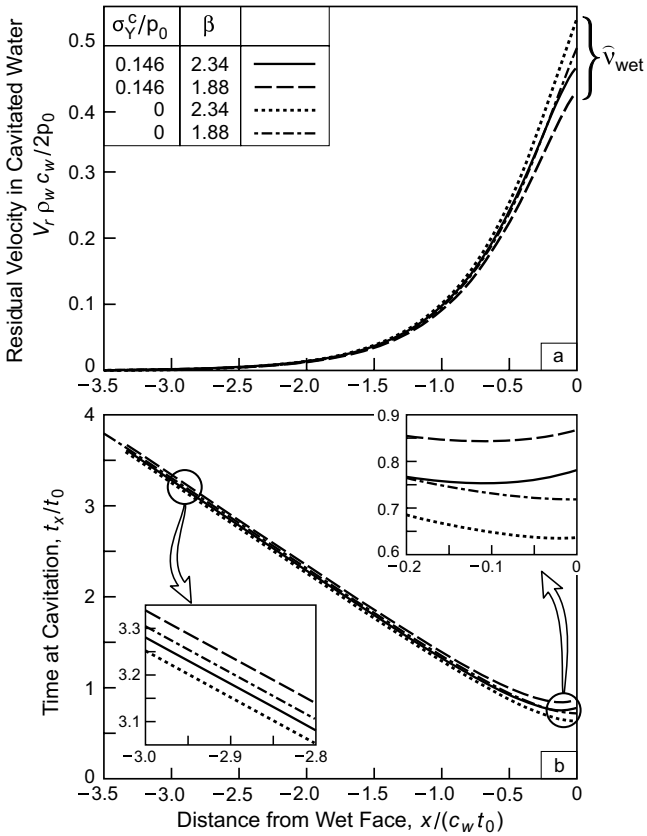

Fig. 5. Analytical predictions of the spatial variation of (a) the residual velocity in the cavitated water at $t = t_c$ and (b) the time to cavitation. These results are for case II in Table 1. Two choices of a time invariant core strength, σ_{YD}^c, and two choices of an effective wet face mass are used, with the wet face mass choices giving β values of 2.34 and 1.88.

noticeable adjacent to the face (Fig. 5a). The variance from the Taylor result for a given wet face mass is at most 15%. Accounting for the core mass by the lumped approximation, or neglecting it completely, produces variations of less than 10%. The time at which cavitation takes place is similarly insensitive to the parameters utilized in the model (Fig. 5b). Note that the cavitation time is linear in x, except very close to the wet face: such that, remotely, $dt_x/dx \approx -1/c_w$, and the cavitation front then moves at its slowest, slightly greater than the sonic speed in water. Since the cavitation pool spreads rapidly relative to the timescale for deceleration (Kennard, 1943), a simple analysis treats t_x as constant and equal to t_c. This insight facilitates the linearization used in Appendix B.

3.4. Sensitivity of predictions for strong and soft cores

The study is continued with comparisons between exact solutions to the analyses of Sections 3.1 and 3.2 and the approximate expressions derived in Appendix B that have been made using the cases outlined in Table 1. The core strength, σ_{YD}^c, is taken to be time invariant, and fixed at the value given by σ_{pulse} as listed in Table 1. Attention is restricted to the time t_c at which cavitation occurs at the wet face and its velocity $\widehat{v}_{wet}$ at that instant. These parameters are the most important, since they form the initial conditions for the stage where reconstitution of the water occurs at the wet face. These comparisons are made with M_{wet} given by Eq. (4a) and the results are summarized in Table 2. The columns labeled 'exact' give results obtained as $\widehat{v}_{wet} = v(0, t_c)$ by the solution of Eqs. (7) and (8) while those labeled Eqs. (B3) and (B4) refer to asymptotic values to first order in σ_{YD}^c/p_0. The Taylor results correspond to the analysis of Section 3.1 with $\sigma_{YD}^c = 0$ which then reduces to

Table 2
Parameters for the analytic model

	t_c/t_0			$\widehat{v}_{wet}\rho_w c_w/2p_0$			$\widehat{v}_{peak}\rho_w c_w/2p_0$
	Exact	Eq. (B3)	Taylor	Exact	Eq. (B4)	Taylor	Eq. (11)
I	0.76	0.75	0.72	0.47	0.47	0.49	0.47
II	0.87	0.83	0.72	0.42	0.43	0.49	0.43
III	0.53	0.52	0.49	0.59	0.59	0.61	0.59
IV	0.74	0.74	0.72	0.48	0.48	0.49	0.48

Exact results obtained by iteration and asymptotic results accurate to first order in σ^c_{YD}/p_0 are provided for t_c (Eq. (B3)) and $\widehat{v}_{wet}$ (Eq. (B4)). Predictions for these two parameters when the core is strengthless are also given in the 4th and 7th column as the Taylor result. The result for $\widehat{v}_{peak}$ from Eq. (11) is exact. All results are obtained with $\beta = \rho_w c_w t_0/M_{wet}$, i.e. the wet face mass includes half the core mass.

$$\frac{t_c}{t_0} = \frac{\ln \beta}{\beta - 1} \tag{16a}$$

and

$$\frac{\widehat{v}_{wet}\rho_w c_w}{2p_0} = \beta^{1/(\beta-1)}. \tag{16b}$$

It is apparent from Table 2 that, for all soft cores (cases I, III and IV), the Taylor results provide sufficient fidelity for both t_c and $\widehat{v}_{wet}$.

For the strong core (case II), the discrepancy in t_c is perhaps problematic and worse than appears from Table 2. The relevant measure to consider is $t_{pulse} - t_c$, since this is the later duration of the high strength stage (with push back stress, σ_{pulse}). If there is a sizable discrepancy in this duration, the influence on the decelerating wet face is large. The Taylor result gives a 14% error. However, it is apparent from Table 2 that the asymptotic values of $\widehat{v}_{wet}$ from (B4) are quite accurate in all cases. Moreover, $\widehat{v}_{peak}$ from Eq. (11) is another good estimate of $\widehat{v}_{wet}$, suggesting that consistent with the Taylor (1963) estimate, cavitation occurs at the wet face approximately when it acquires its peak velocity.

It is also of interest to examine the fidelity of the models during deceleration of the wet face. In order to facilitate such a comparison we consider a plate of mass $M_{wet} = 80\ \text{kgm}^{-2}$ on a massless plastic foundation of time invariant strength $\sigma^c_{YD} = 14.6$ MPa. This plate is loaded by a water blast of the form (5) with $p_0 = 100$ MPa and $t_0 = 0.1$ ms, and the resulting velocity of the plate, v_{wet}, as a function of time, t, is plotted in Fig. 6. The parameters used in these calculations are representative of case II of Table 1. Predictions of three sets of analyses are presented in Fig. 6 as follows:

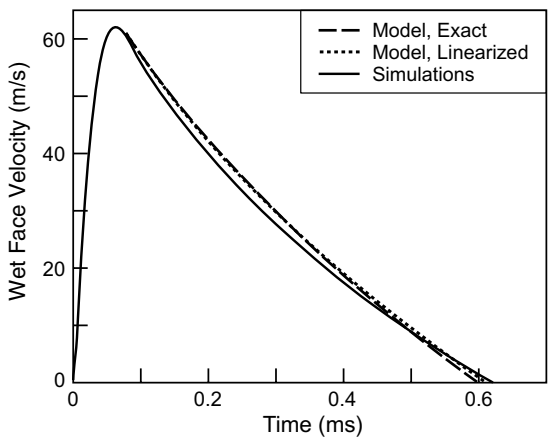

Fig. 6. Analytical (exact and linearized) and FE predictions of the temporal dependence of the wet face velocity for a plate of mass $M_{wet} = 80\ \text{kgm}^{-2}$ on a plastic foundation of strength $\sigma^c_{YD} = 14.6$ MPa impinged by a water blast wave with peak pressure $p_0 = 100$ MPa and $t_0 = 0.1$ ms.

(i) The exact solution to the equations presented in Section 3.1 and labeled as the exact model in Fig. 6.
(ii) The predictions of the linearized equations of Appendix B.
(iii) Predictions of finite element (FE) simulations.

Details of the fluid–structure interaction finite element simulations are provided in Section 4. Here it suffices to clarify that, unlike in the analytical models, in the finite element simulation for Fig. 6, the wet face is modeled as an elastic material with density and elastic properties representative of steel and thickness 10 mm (so as to give $M_{\mathrm{wet}} = 80\ \mathrm{kgm}^{-2}$). The strength of the core is modeled by a traction boundary condition on the plate's dry side, set at zero until motion commences there, and jumping thence to 14.6 MPa. The good agreement between the model and FE simulations (Fig. 6) affirms the fidelity of the model and the linearized version of the predictions presented in Appendix B.

4. Finite element assessment

The three-dimensional numerical model has been described by Liang et al. (2007). It consists of a water column above the wet face. Contact is enforced at the interface between the water and the panel, and the free-standing sandwich plate is modeled via symmetry boundary conditions as depicted in Fig. 7. A uniform pressure boundary condition is imposed on the top surface of the water column. The commercial code, ABAQUS/Explicit (2006), is used. Eight-node three-dimensional brick elements with reduced integration (C3D8R) are employed to model the water, while four-node shell elements (S4R), with five integration points through the thickness, are used to model the faces and the core members. The water is assumed to be linear elastic under compression, with zero tensile strength and zero shear modulus, such that $\rho_{\mathrm{w}} = 1000\ \mathrm{kgm}^{-3}$ and $c_{\mathrm{w}} = 1500\ \mathrm{ms}^{-1}$.

All calculations are performed for unit cells of fixed mass per unit area, $m_{\mathrm{total}} = m_{\mathrm{wet}} + m_{\mathrm{dry}} + m_{\mathrm{core}} = 160\ \mathrm{kgm}^{-2}$, corresponding to a solid plate thickness, $H_{\mathrm{eq}} = 2$ cm. This choice lends consistency with prior assessments by Xue and Hutchinson (2004) and Liang et al. (2007). The cores have thickness in the range $0.1\ \mathrm{m} \leqslant H_{\mathrm{c}} \leqslant 0.3\ \mathrm{m}$. The I-core configuration is used with dimensions that allow both strong and soft responses to be probed. The core relative density is varied in the range $1.3\% \leqslant \bar{\rho} \leqslant 4\%$, and the ratio of dry to wet face thickness is $1 \leqslant h_{\mathrm{dry}}/h_{\mathrm{wet}} \leqslant 4$ (Liang et al., 2007). The spacing between the webs of the I-core is 0.1 m. The impulses used all have decay time $t_0 = 0.1$ms and pressure in the range $100\ \mathrm{MPa} \leqslant p_0 \leqslant 200\ \mathrm{MPa}$. The material properties are representative of those for 304 stainless steel, elaborated by Stout and Follansbee (1986), Liu and Guo (2000) and Zok et al. (2004). They include strain and strain-rate hardening with an effective plastic wave velocity of $c_{\mathrm{pl}} \approx 1\ \mathrm{kms}^{-1}$. A previous assessment by

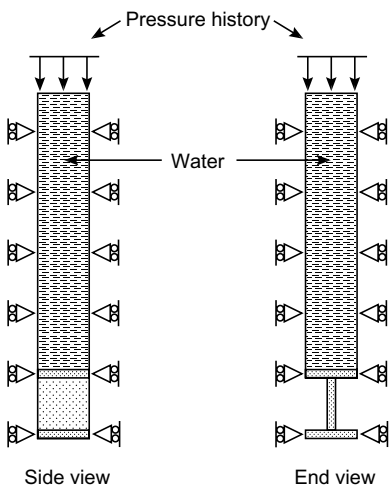

Fig. 7. A sketch of the boundary conditions employed in the analysis of a free-standing sandwich plate impinged by a water blast.

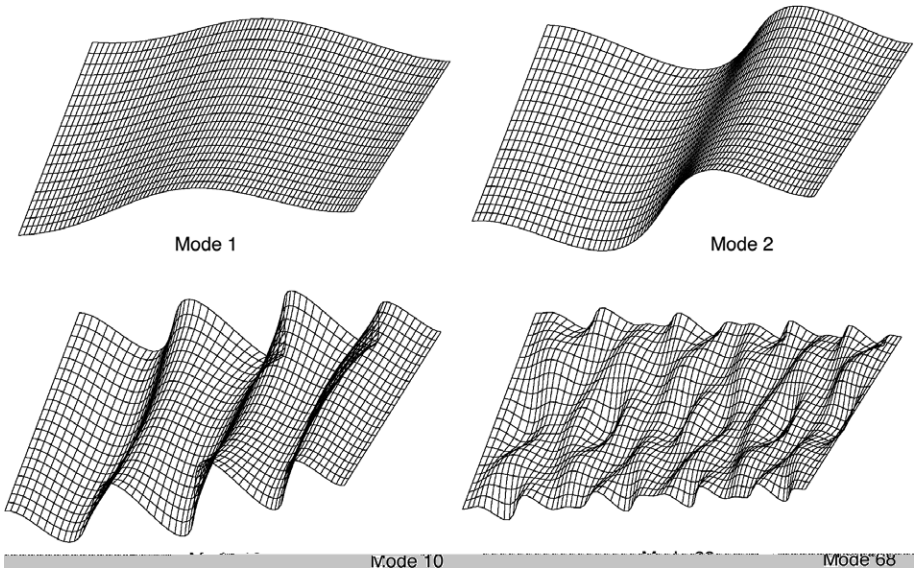

Fig. 8. The combination of shapes used for the core needed to capture the buckling modes of a 304 stainless steel I-core panel observed by Ferri et al. (2006).

Ferri et al. (2006) has provided input about the importance of imperfections in the core member. The essential result is that, to capture the buckle-wave dynamics effectively (Vaughn and Hutchinson, 2006), imperfections are required with a combination of eigenmodes. A representative combination is depicted in Fig. 8, and the amplitude of each eigenmode imperfection can be found in the work of Ferri et al. (2006). In these three-dimensional FE simulations, the wet and dry faces do not have spatially uniform velocities and hereafter, for the FE calculations, we define v_{wet} and v_{dry} as the velocities of the wet and dry faces averaged over the respective faces. The component of velocity in the vertical direction in Fig. 7 is averaged, so that the vertical momentum of the face is correctly represented by the averaged velocity.

Results for the time variation of v_{wet} and v_{dry} are presented for the four cases considered in Sections 3.3 and 3.4 as listed in Table 1. From a preliminary comparison (Fig. 9), it is apparent that cases I, III and IV have a soft response: the wet face velocity always exceeds that of the dry face (Fig. 1). In contrast, case II exhibits a strong response such that the two face velocities equalize, at $t_{\mathrm{common}} \approx 0.7$ ms. To demonstrate that extra momentum is acquired from the cavitated water, a comparable case I result is obtained by imposing an initial wet face velocity equal to $\widehat{v}_{\mathrm{wet}}$ (67.1 m/s), but without the water (Fig. 10), i.e. an impulsive load.

5. Comparison with analytic model

5.1. Core characterization using dry face velocities

Comparisons between the face velocities obtained by finite elements and analytic estimates are included in Fig. 9. The bimodal response of the core is most apparent in the dry face velocity. For example in case I (Fig. 9a), at short times, $t < t_{\mathrm{pulse}}$, the acceleration is rapid and constant with $\dot{v}_{\mathrm{dry}} = 56\ \mathrm{kms}^{-2}$. Thereafter, at t_{pulse}, there is an abrupt change: whereupon the acceleration reduces to, $\dot{v}_{\mathrm{dry}} = 4\ \mathrm{kms}^{-2}$. The characteristic time is $t_{\mathrm{pulse}} = 0.31$ ms. The corresponding times for all other cases are summarized on Table 1. These differing accelerations are directly connected with the two levels of core strength. With employment of Eq. (14), the effective dynamic strength of the core can be ascertained, before and after t_{pulse}, as σ_{pulse} and σ_{ss}, respectively. Note that there is some leeway in the fitting of constant accelerations to the finite element results for the motion of the dry face, and judgments have to be made. The resulting estimates of the core strength are presented in Table 1 and the consequent analytical predictions of the dry face velocities, obtained by integrating